Arabian Journal for Science and Engineering (2022) 47:9345–9359
https://doi.org/10.1007/s13369-021-05600-z

RESEARCH ARTICLE-COMPUTER ENGINEERING AND COMPUTER SCIENCE

Upgrading the Quality of Power Using TVSS Device and PFC Converter Fed SBLDC Motor

U. Arun Kumar[1] · **C. S. Ravichandran**[2]

Received: 13 November 2020 / Accepted: 24 March 2021 / Published online: 20 April 2021

Abstract
This globe has now come to a point where it is unmanageable for humans to do any work without power. Therefore, the main motive of this paper is to ameliorate the status of power. So to boost the condition of power, there are three predominant processes. So this proposed procedure performs functions like repressing the transitory voltage surge, get unification of PF, and lowering the harmonic distortion. This is because power changes, whether high or low, present a complication with electrical equipment. Therefore, transient voltage surge suppressors are utilized in the AC power line to stay the power changes usual. Then, for the motive of unifying the energy factor and lessening the harmonic distortion, this paper utilizes the more efficient BLDC Motor fed through bridgeless converter configuration. Because utilizing a brushless motor, performs functions extremely efficiently such as longevity, increasing reliability and reduced noise. However, since it is exceeding principle to command the speed of the motor, the Sensorless form is utilized here. The intention of utilizing this is the spot of the rotor is extremely pivotal to handle the momentum of the motor and it's also hugely difficult to identify. Therefore, this proposed mechanism for performing these functions utilizes the Sensorless BLDC Motor and to reach power factor correction (PFC) bridgeless converter topologies are used. A comparitive analysis is done among the various converters and the best converter is analyzed based on the PQ parameters. The obtained quality of power is under the acceptable limits of IEEE and IEC standards.

Keywords Improved power quality · TVSS device · Sensorless brushless DC (SBLDC) motor · Power factor correction (PFC)

1 Introduction

Nowadays brushless motors are utilized additional often than brushed motors. The reason is that brushless motors are very good performing at the low sound noise and power efficiency improvements. Usually brushless motors use one or more sensors. With this function, the sensor is wired and the cost of operating it is high. Also, sensors cannot be used in rotor existing applications in closed housing. In applications where the motor is submerged in a fluid such as a compressor, or some pumps, must keep the number of electrical inputs to a minimum. So in terms of technology and cost reason, Sensorless BLDC Motor is considered as a major requirement. This Sensorless BLDC Motor gives very high performance, at very low cost. As a result of high performance, excessive torque to inertia ratio, excessive power density, low preservation need and extensive variety of speed manipulate; brushless DC (BLDC) motors are extensively favoured in lots of minimal and medium energy exeercises. It's far used in many house equipments of Gadget like fans, air conditioners, water pumps, Refrigerators, washing machines etc.It also finds applications in lots of commercial gear, medical equipments, Heating, air flow and air con, robotics and Particular movement control structures [1–3].

✉ U. Arun Kumar
arunkumarukce@gmail.com

C. S. Ravichandran
eniyanravi@gmail.com

[1] Department of Electrical and Electronics Engineering, Kathir College of Engineering, Coimbatore, Tamilnadu 641062, India

[2] Department of Electrical and Electronics Engineering, Sri Ramakrishna Engineering College, Coimbatore, Tamilnadu 641022, India

In the last decade, bridgeless configurations gained more importance due to reduced switching losses and improved PFC at AC mains. This is achieved by eliminating the DBR partially [4]. Conventional bridgeless configuration includes boost converter configuration which reduces the common mode noise. In paper [1], BL-BBC has been used. It is utilized to improve the level of energy, and in which Hall Effect sensors have been utilized. In paper [2], BL-CSCC has been utilized to progress the PF with usage of least number of components and conducting devices. This configuration exhibits the minimum conduction losses due to reduced component conduction in both the cycles. In paper [3], BL-CC is utilized to boost or raise the status of the power with a very simple voltage follower approach. This paper is mainly utilized in air conditioning applications and with applications of reduced sensors.

In paper [5], the BL-LC is utilized to raise the energy factor, and in which a one only sensor has been utilized to improved the PF. Moreover, the switching losses of the VSI is minimum with wide range of speed control. Also the switching stress is reduced comparatively with other bridgeless configurations. In paper [6], the LUO converter is utilized to improve the PFC which is a low cost solution for all low power applications. Also, LUO converter is widely used in many voltage lifting applications. In paper [4], the BL-SEPIC Converter is utilized to promote the PFC and speed control of brushless drive. The performance of this configuration is satisfactory for speed control and supply fluctuations with reasonable switching losses. In paper [7], the BL-ZC is used to attain a power factor close to unity at supply mains; It includes a single voltage sensor for speed control and PFC. In paper [8], the hysteresis comparator has been used to operate the BLDC motor without a sensor. Usage of this converter provides proper commutation pulses to the inverter and the presence of LPFs compensates the phase lag of back EMF which produces significant pulsating torques which in turn causes load disturbances.

Normally hall sensors will be used to get the alignment of rotor position for commutation purpose. Here in the poposed design hall sensors are removed and a sensorless control technique is proposed [9]. Although, position sensors are used to achieve noiseless torque, due to the immunity level and reduced consistency the position sensors are removed by implementing a sensorless control design. Usually, back emf estimation design will be used which is also termed as teminal voltage estimation technique provides the position of rotor with low amplitude [8]. To avercome this align and go techniques is used. Other SBLDC techniques like third harmonic terminal voltage technique and PLL are developed but leading to noise and interference problems which makes the commutation more difficult [9]. Also zero crossing point estimation techniqes has been suggested by researchers by using V and I sensors. To avoid the above said blemishes a hysteresis comparator technique is used with applicable high starting torque. Therefore, this paper presents a power quality improvement scheme using SBLDC motor with hysteresis comparator technique [8]. So in this proposed methodology, five types of converters with a voltage follower approach is used and fed to SBLDC motor with hysteresis comparator technique and then a comparison is

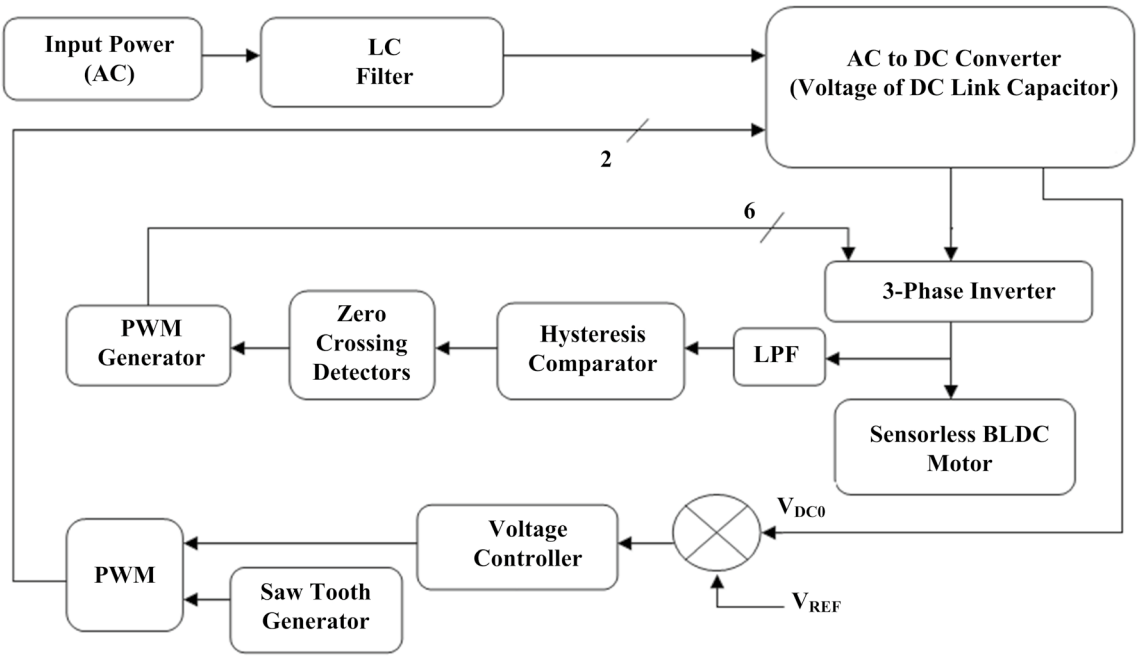

Fig. 1 Flow of this proposed method

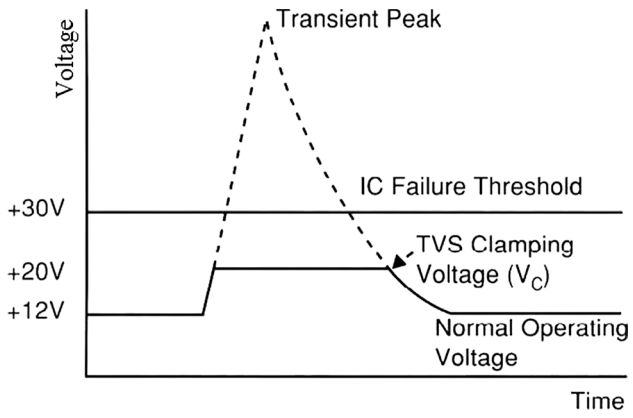

Fig. 2 Diagram of clamping voltage

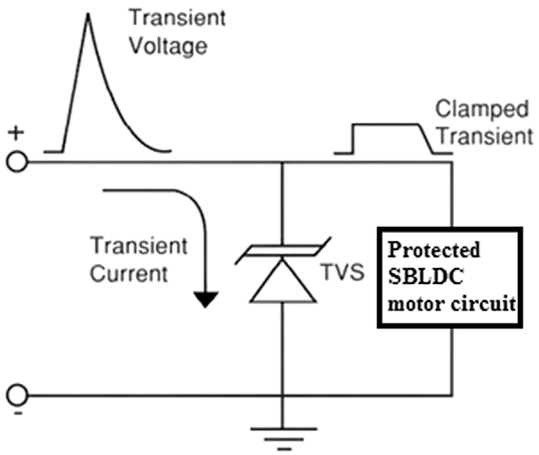

Fig. 3 TVS circuit diagram

done with the output parameters. Finally, a better converter configuration is identified for achieving better power factor and efficiency.

2 Proposed Methodology

In this proposed method, the AC to DC converters are utilized to wield the BLDC motor to improve PF in the supply mains, AC Supply is fed through LC Filter and to the AC-DC converter. The AC to DC converters which converts the AC to the required level of DC. It is then provided to VSI having six-stage switches. This paper uses the hysteresis comparator for sensorless control. This comparator incorporates the LPF to suppress high switching frequency ripples. Hysteresis comparator is utilized to create gating signals to the VSI. The gating signal generator is utilized to generate six PWM signals. The voltage across dc link capacitor is taken to the voltage controller and compared with the reference voltage. The voltage controller then turns them into a constant voltage and gives it to PWM. This is then compared with sawtooth generator and the input PWM is given to the AC to DC converter. Usage of hybrid controller improves the robustness of the system and suppresses the chattering of the load. Furthermore, design of hybrid controller can provide desirable performance which is not possible with linear control technique. [9–15] (Fig. 1).

2.1 TVS

Transients are temporary changes in frequencies. TVS device is a component that can protect and isolate circuits. It is utilized to filter and control an unstable and high voltage. This makes it possible to keep the VSI fed SBLDC circuit very secure. In the hardware part, this TVS device shall provide excellent surge protection to the 6-pack VSI Fed SBLDC. This, in turn, distorts or reverses the voltage spike from the circuits of the SBLDC motor. This means that if an instant enlarge in voltage is greater than three nanoseconds, the voltage fluctuation will occur. This, in turn, will attack the circuitry of the SBLDC motors. If the spike is sudden crossing over, then the PN junction is back to normal. Then, when comes to the next spike, the spike will hold tight. In normal function, the TVS are invisible to the round to be protected. Here may need to install a high voltage surge or a device that absorbs unnecessary heat to TVS. Generally, the peak power flowing through the TVS is handled in the kilowatt range.

In Fig. 2, on the y-axis, the voltage exceeds the 20 V upper limit. Then the TVS accept that high voltage range and responds immediately to that. TVS diodes protect the circuits from Electrostatic Discharge (ESD). Here TVS secures a signal chain in one direction. Thus, it allows the signal chain to only flow at the top. This means that the TVS defend the input power of the circuit [16–20] (Fig. 3).

Typically the V_{MW} is below 10–15% the V_B. The voltage that TVS devices go into avalanche is called V_B. Temperature affects V_B size. Thus, the V_{MW} is at least 10% lower than the V_B. This is because when the temperature drops, the flow of V_B is less. TVS should not have a breakdown voltage equal to the working peak voltage. The clamping voltage is the highest voltage in the TVS. The V_C is 60% greater than the V_{MW} and the 35–40% higher than the V_B.P_{PP} dispersion is one of the factors to safely suppress various upheavals or ratings. Therefore,

$$P_{PP} = V_C \times I_{wcs}$$

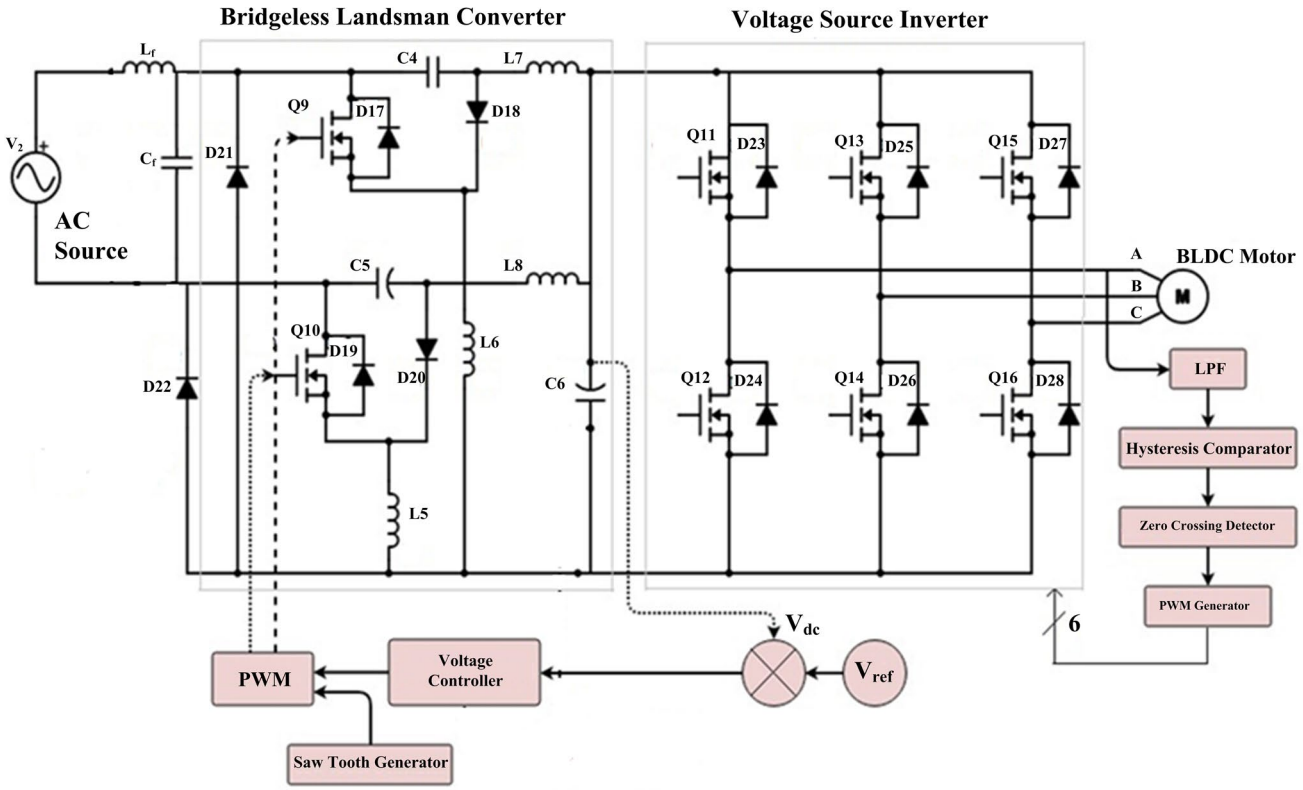

Fig. 4 Circuit diagram of BL-LC

where V_B = breakdown voltage, V_{MW} = maximum working voltage, V_C = clamping voltage, P_{PP} = peak pulse power, I_{wcs} = worst-case surge current.

2.2 AC to DC Converter

Five types of AC to DC converters are utilized in this present method. Then, which of these 5 converters are found to be the best. The 5 types of schemes of AC–DC converters are given below:

1. Bridgeless landsman converter (BL-LC)
2. Bridgeless cuk converter (BL-CC)
3. Bridgeless buck-boost converter (BL-BBC)
4. Bridgeless zeta converter (BL-ZC)
5. Bridgeless canonical switching cell converter (BL-CSCC)

2.3 BL-LC

In Fig. 4 in which the converter balance on both Discontinuous Inductor Current Mode (DICM) and Continuous Inductor Current Mode (CICM).The converter manipulates in the Positive Half Cycle (PHC) and Negative Half Cycle (NHC) of the AC distribution fewer than three distinct systems. Here the functionality of the converter is described in each mode:

Mode 1 When the switch Q9 is attached by a gate signal, the energy from the mains is sent to the capacitor C4 input inductance L6 along with the stored charge. The inductor starts charging, the output inductor begins to settle. The output capacitor C6 begins to charge due to the ejection of the capacitor C4. Consequently the voltage V_{dc} over the output capacitor begins to increase.
Mode 2 After switch Q9 switch is off, output inductor L7 and capacitor C4 are supplied with energy from the supply mains. So C4 and L7 start charging, begin to discharge the inductor L6, then the energy is delivered from the capacitor C4 to the motor.
Mode 3 In this practice the converter works in DICM. In this method the input inductor L6 is completely eliminated and then the energy is zero in the inductor. The charge from the output inductor L7 is caring to the DC Link capacitor C6. Thus, when the converter is running at the DICM, a series of supply for the motor is also maintained.

In DICM, the BL-LC is designed to function. In standard, the DC bus voltage is essential in the ink for speed control from 12 V/V_{dcmn} to 24 V/V_{dcmx}. This is set as V_{sc} in and below equation:

$$V_{sc} = V_{pk}\mathrm{Sin}\,(2\pi f_{li}t) \tag{1}$$

The median rectified i/p voltage V_i is modeled as given in Eq. (2).

$$V_i = \frac{2\sqrt{2}V_{sc}}{\pi} \tag{2}$$

The BL-LC duty rate D_R is expressed in Eq. (3).

$$D_R = \frac{V_{dc}}{\left|V_p\mathrm{Sin}(\omega t)\right| + V_{dc}} \tag{3}$$

where V_{dc} and V_{pk} are the peak input voltage, voltage across the output capacitor and angular frequency, respectively. The output for output inductors with allowable ripple current (Δi) is given in Eq. (4),

$$\mathrm{L7,\ 8} = \frac{1}{\Delta i f_a}\left(\frac{V_{sc}^2}{P_i}\right)\left(\frac{V_{dc}}{V_i + V_{dc}}\right) \tag{4}$$

Using Eq. (5), the critical value of the i/p inductors L_{ci} is derived,

$$L_{ci1,2} = \frac{V_{sc}^2}{P_i}\frac{V_{dc}}{2V_i f_a}\left(\frac{V_{dc}}{V_i + V_{dc}}\right) \tag{5}$$

To manage in DICM, the values of the input inductors L5, 6 are smaller than the critical value $L_{ci1,2}$. Equation 6 is utilized to frame the values of the intermediate capacity.

$$C4,\ 5 = \frac{V_{dc}}{K\left(V_{dc} + V_i\right)f_a\left(\frac{V_{dc}^2}{P_i}\right)}\left(\frac{V_{dc}}{V_i + V_{dc}}\right) \tag{6}$$

Here the DC connector, the ripple inclusions of the voltage across the capacitor is introduced to as K. The value of the DC connector capacitor is designed to be Eq. (7),

$$C_{dc} = \frac{P_i}{2\omega\Delta V_{dc}^2} \tag{7}$$

In Eq. (8), the limit for maximum filter capacity C_{fmx} is given. I_s and V_s reveal the peak value of V and I. The phase variation betwixt the I_S and V_{sc} is indicated by theta, and it is selected as 1°.

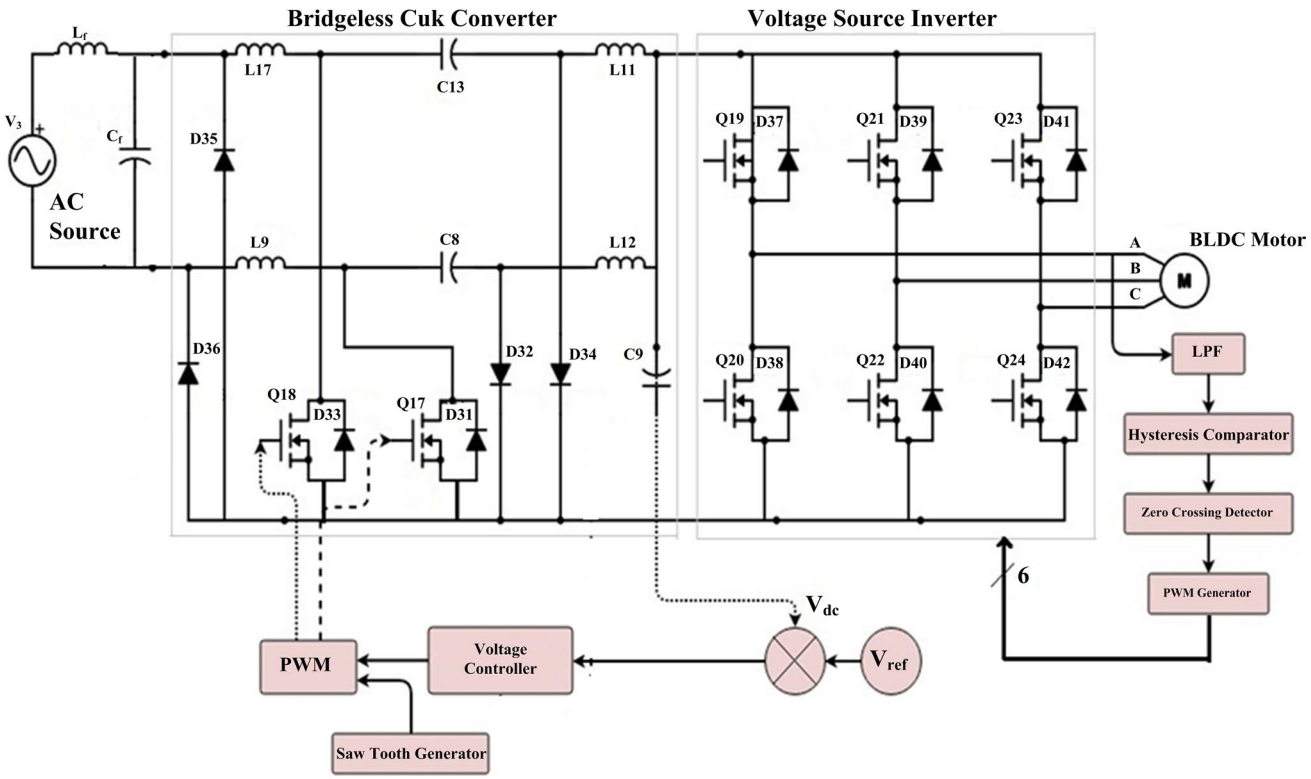

Fig. 5 Circuit diagram of BL-CC

$$C_{\mathrm{fm}} = \frac{\left(\frac{\sqrt{2}P_{\mathrm{m}}}{V_{\mathrm{sc}}}\right)}{\omega_{\mathrm{L}}\, V_{\mathrm{sc}}} \tan(\theta) \tag{8}$$

Capacitance in the filter has a selective value, rather than that of C_{fm}. From Eq. (9), the filter inductor Lf is estimated. LPF between the $f_{\mathrm{l}} < f_{\mathrm{co}} < f_{\mathrm{sw}}$ is designed to have a cut-off frequency f_{co}.f_{co} has been chosen as 2000 Hz. The reason why this value is so high is to accommodate a minor amount of stimulation. By Eq. (9), the value required for inductor in the filter is calculated.

$$L_{\mathrm{f}} = L_{\mathrm{r}} + 0.04\left(\frac{1}{\omega_{\mathrm{L}}}\right)\left(\frac{V_{\mathrm{sc}}^2}{P_{\mathrm{o}}}\right) \tag{9}$$

2.4 Bridgeless Cuk Converter

The converter here is designed to operate in DICM as shown in Fig. 5. In this event, when the current of the output inductor L11 and L12 is steady, the voltage across the transitional capacitors Vc13 and Vc8 and the current in the input inductor L17 and L9 continue to reach a PFC in the mains. The AC distribution has both PHC and NHC. The switch Q18 is transfer and via L17 and D36 to the PHC of the supply voltage. The energy is relocating via the energy transfer capacitor C13, L11 and D34. Likewise for the NHC of the supply voltage, the switch Q17 handles L9 and D35. A regular DC connector is utilized for the NHC and PHC of the capacitor C9 justification. DC connector capacitors C9 are utilized to attain the pace of the BLDC motor. The various modes of operation are explained below:

Mode 1 During the switch Q18 is turned on, the energy is gathered in the i/p inductor L17 via the diode D16. Inductor current iL17 improves. Also the power stored in the intermediate condenser C13 is dispensed to the output inductor L11 and DC link capacitor C9. So the DC link voltage V_{dc} and current iL11 are improved, throughout the voltage of the intermediate capacitor Vc13, this function mode decreases.

Mode 2 When switching off the switch Q18, the inductor discharges through the intermediate capacitor C13 exits through the diode D34 and D36. Inductor L11 then converts its stored energy to the DC-link capacitor C9, So in this function routine, the current of the inductors L17 and L11 persistent to lessen. At the similar time, the voltage of the intermediate condenser C9 and the DC coupling capacitor C13 is increased.

Mode 3 In this mode there is no energy in the inductor L11 of the output, that is, iL11 = 0. Input inductor iL17 raises the voltage of the intermediate capacitor C13. At this time, the DC connection provides the energy required for the capacitor C9. So the V_{dc} is reduced. This operation continues until the switch Q18 is switched on again.

The input average voltage is given in equation below:

$$V_{\mathrm{iavg}} = \frac{2\sqrt{2}V_{\mathrm{sc}}}{\pi} \tag{10}$$

The BL-CC DC connector is designed from V_{dcmn} to V_{dcmx} for voltage control. Below is the Duty Rate (DR) for the BL-LC:

$$\mathrm{DR} = \frac{V_{\mathrm{dc}}}{V_{\mathrm{dc}} + V_{\mathrm{iavg}}} \tag{11}$$

Hence the DR is for designed (d_{d}), maximum (d_{mx}) and minimum (d_{mn}) corresponding to V_{dcd}, V_{dcmx} and V_{dcmn} are calculated. Now the nominal DR (d_{n}) is taken less than d_{d} for an efficient control in DICM, equation of both inductors L17 and L9,

$$\mathrm{L17} = \mathrm{L9} = \frac{V_{\mathrm{p}} d_{\mathrm{n}} T_{\mathrm{sw}}}{\Delta i_{\mathrm{Li}}}$$

where V_{p} = peak of supply voltage, T_{sw} = switching period, f_{sw} = switching frequency.

The important conduction parameter K_{ic} equation,

$$K_{\mathrm{ic}} = \frac{1}{2\left\{\left(\frac{V_{\mathrm{dcd}}}{V_{\mathrm{p}}}\right) + n\right\}^2} \tag{13}$$

The conduction parameter K_{c} for the function in DICM,

$$K_{\mathrm{c}} < K_{\mathrm{ic}} \tag{14}$$

Equivalent inductive L_{e} calculation,

$$L_{\mathrm{e}} = \frac{R_{\mathrm{el}} T_{\mathrm{sw}} K_{\mathrm{c}}}{2} = \frac{\left(\frac{V_{\mathrm{dcd}}^2}{P}\right)\left[\frac{1}{f_{\mathrm{sw}}}\right] K_{\mathrm{c}}}{2} \tag{15}$$

Here, R_{el} = equivalent load resistance. The equation for the value of the o/p side inductor,

$$\mathrm{L11} = \mathrm{L12} = \frac{L_{\mathrm{in}} L_{\mathrm{e}}}{L_{\mathrm{in}} - L_{\mathrm{e}}} \tag{16}$$

The estimation for the capacity of energy transfer capacitors is,

$$\mathrm{C13} = \mathrm{C8} = \frac{1}{\omega_{\mathrm{re}}^2 \left[L_{\mathrm{in}} + L_{\mathrm{ou}}\right]} \tag{17}$$

where $\omega_{\mathrm{re}} = 2\pi f_{\mathrm{re}}$, f_{re} = the resonant frequency and $f_{\mathrm{sw}} > f_{\mathrm{re}} > f_{\mathrm{li}}$ where f_{li} = the line frequency. The equation of the value of the DC connecting condenser is as follows,

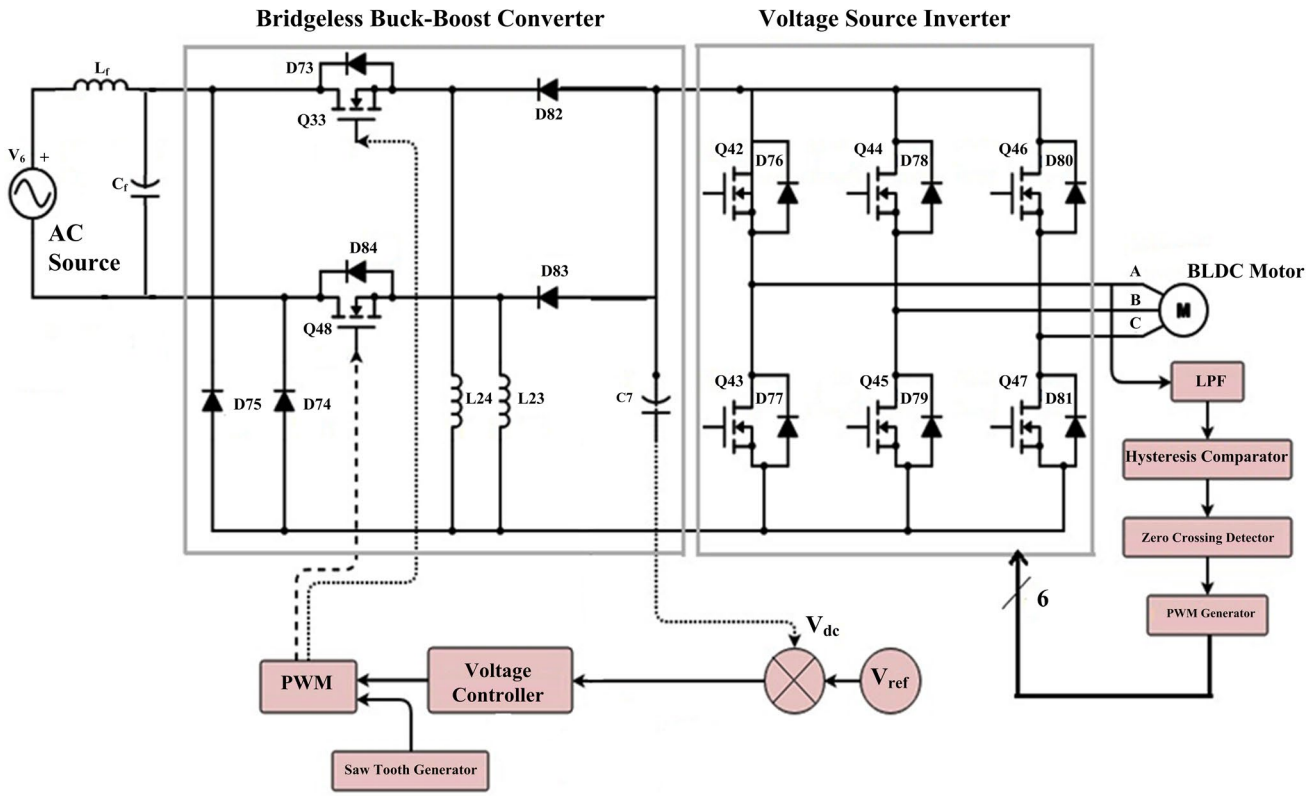

Fig. 6 Circuit diagram of BL-BBC

$$C_{\mathrm{dc}} = \frac{I_{\mathrm{dc}}}{2\omega_{\mathrm{li}}\Delta V_{\mathrm{dcc}}} \tag{18}$$

where I_{dc} = DC couple current, ω_{li} = line frequency, ΔV_{dcc} = permitted ripple voltage in DC pairing condenser.

The sum of the maximum value of the filter is,

$$C_{\mathrm{fmx}} = \frac{I_{\mathrm{p}}}{\omega_{\mathrm{li}} V_{\mathrm{p}}} \tan(\theta) \tag{19}$$

2.5 BL-BBC

The behavior of the BL-BBC is partitioned into 2 types. This comprises the activity of the PHC and NHC of the supply voltage and the thoroughgoing switching cycle, Switches Q33 and Q48 in this BL-BBC handle in the PHC and NHC. For the PHC, 3 styles of workable during the proper transition cycle are discussed. The workable of those three methods is detailed below (Fig. 6).

Mode 1 This practice is utilized Q33 to charge L24. In this process the inductor current iL24 is increased. The diode D74 consummates the input side circuits. Then the DC connector is discharged by the capacitor C7.

Mode 2 In this form of performance, switch Q33 is switches off, the energy is collected in the inductor L24 is relocated to the DC-link capacitor C7 until the trigger is absolutely discharged. The current in the inductor L24 dwindles and then reaches zero.

Mode 3 In this mode, the inductor L24 enters into non-stop conduction. That is, there is no charge in the inductor. Hence the current iL24 becomes zero for the remaining transition period. The DC-coupling Capacitor C7 delivers energy. So the DC connection reduces the voltage V_{dc} across the capacitor. After a proper switching cycle, the operation is redo when the switch Q33 is turned on.

The equation for computing the median current is in Eq. (2). Equation of voltage conversion rate is in Eq. (11). The inductor L_{ci1} values equation to act as the critical conduction manner in the BBC converter,

$$L_{\mathrm{ci1}} = \frac{R_{\mathrm{el}} 1 - (\mathrm{DR})^2}{2f_{\mathrm{sw}}} \tag{20}$$

Now, L_{ci1}'s value is calculated at the worst duty rate in d_{mn}. The equation corresponding to V_{dcmn} the value of the inductor L_{cimn} is given below,

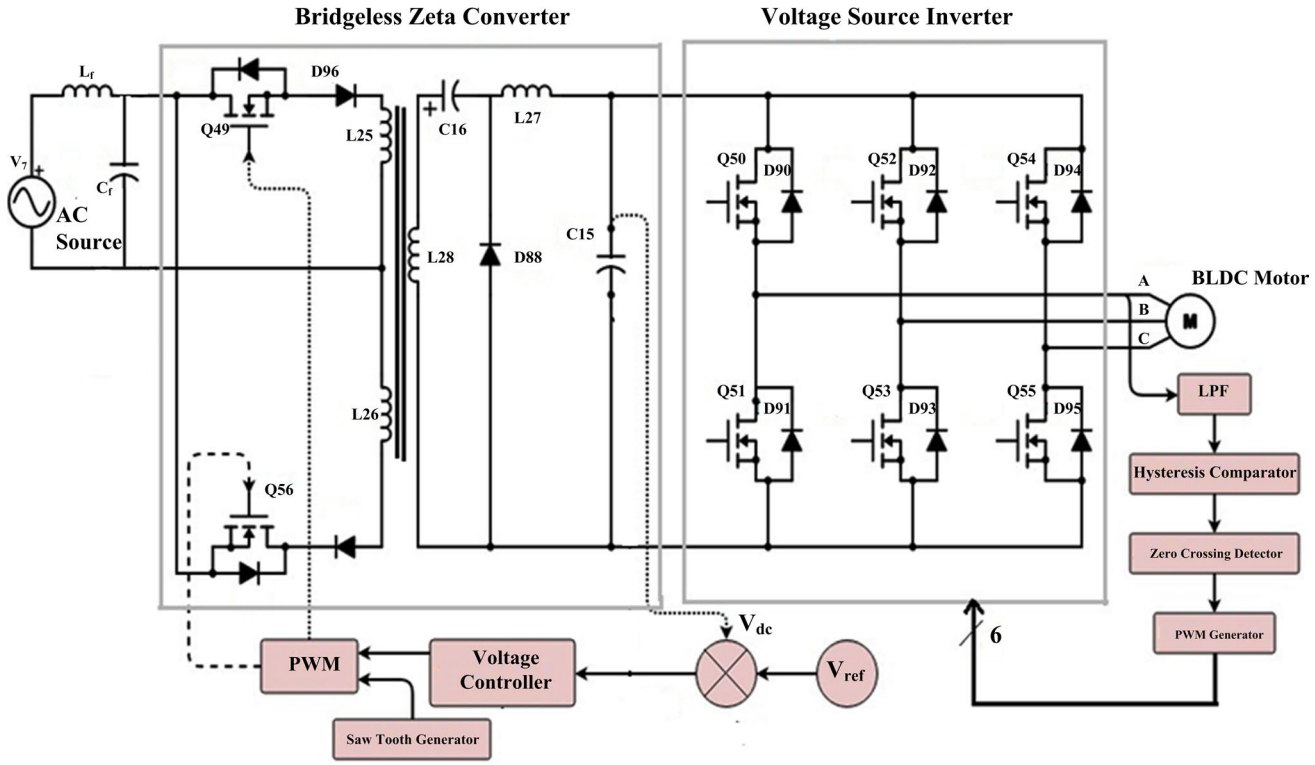

Fig. 7 Circuit diagram of BL-ZC

$$L_{\text{cimn}} = \frac{V_{\text{dcmn}}^2}{P_{\text{mn}}} \frac{1 - d_{\text{mn}}^2}{2f_{\text{sw}}} \tag{21}$$

For the PFC function, the supply current I_{su} is in phase. Calculation of input power P_{i},

$$\begin{aligned} P_{\text{i}} &= \sqrt{2}V_{\text{su}} \sin \omega t . \sqrt{2} I_{\text{su}} \sin \omega t \\ &= V_{\text{su}} I_{\text{su}} (1 - \cos 2\omega t) \end{aligned} \tag{22}$$

The second line corresponds to harmonics; this is mirrored in the DC Link capacitor,

$$i_{\text{c}}(t) = -\frac{V_{\text{su}} I_{\text{su}}}{V_{\text{dc}}} \cos 2\omega t \tag{23}$$

Under is the DC pair voltage ripple associated with this Capacitor Current,

$$\Delta V_{\text{dc}} = \frac{1}{C_{\text{dc}}} \int i_{\text{c}}(t) \text{d}t = -\frac{I_{\text{dc}}}{2\omega C_{\text{dc}}} \sin 2\omega t \tag{24}$$

In DC-incorporating condenser, the voltage to the maximum value, sin (ωt) is taken 1. So its sum is rewritten under,

$$C_{\text{dc}} = \frac{I_{\text{dc}}}{2\omega \Delta V_{\text{dc}}} \tag{25}$$

Now the DC Link capacitor, planned value, in V_{dcd} DC connection voltage, computed with permitted ripple. Equation of dc link condenser is,

$$C_{\text{dc}} = \frac{\frac{P_{\text{ou}}}{V_{\text{dcd}}}}{2\omega \Delta V_{\text{dc}}} \tag{26}$$

2.6 BL-ZC

Similarly for the NHC of the V_{sc}, the current does not flow through the switch and diode. Here the energy is converted by the high frequency transformer (HFT). Its proportion is given as F1: F1: F2, planned to perform as magnetization, in DCM. This is to reach an intrinsic PFC; broad gamut of DC connection middle conduction is reached for voltage control.

There are 3 modes of operations for this converter. One of those operations is, for the PHC of the V_{sc} function during the consummate switching cycle. When switch Q49 is running, the energy is saved in the inductor L27, the HFT and the intermediate capacitor C16. While the DC link Capacitor, The C15 delivers enough power for the load. When the switch is turned off, inductor and diode HFT eject give the power necessary for the DC coupling capacitor. In DCM process manner, HFT is totally eradicated.

Whereas, following the inductor L27 the DC connection provides the energy required for the capacitor (Fig. 7).

The equation of the input voltage V_{sc}, given in an Eq. (1), the input average voltage V_{ia} is considering in the equation below,

$$V_{ia} = \frac{2V_p}{\pi} \tag{27}$$

Output voltage, isolation of the isolated ZC converter is provided by V_{dc}. Equation is,

$$V_{dc} = \left(\frac{F2}{F1}\right)\frac{DR}{(1-DR)}V_i \tag{28}$$

The equation of DR is calculated as,

$$DR = \frac{V_{dc}}{V_{dc} + \left(\frac{F2}{F1}\right)V_i} \tag{29}$$

The value of the equivalent load resistance R_{el} is computed by the next equation:

$$R_{el} = \frac{V_{dc}^2}{P_{ou}} \tag{30}$$

To control on the border of CCM and DCM, HFT's magnetization inductor L_{mc} equation of critical value,

$$L_{mc} = \frac{(1-DR)^2 R_{el}}{\left(\frac{F2}{F1}\right)^2 2Df_{sw}} \tag{31}$$

The value of the magnetization inductor L_{mag} is picking as given below,

$$L_{mag} << L_{mc} \tag{32}$$

The value of the o/p inductor L27,

$$L27 = \frac{V_{ou}(1-DR)}{f_{sw}\Delta i_{L27}} \tag{33}$$

The value of in-between capacitor C16,

$$C16 = \frac{V_{dc}DR}{\Delta V_{ci} R_{el} f_{sw}} = \frac{V_{dc}DR}{V_p R_{el} f_{sw}} \tag{34}$$

The value of the DC coupling capacitor is given below,

$$C_{dc} = \frac{I_{dc}}{2\omega_{li}\Delta V_{dc}} \tag{35}$$

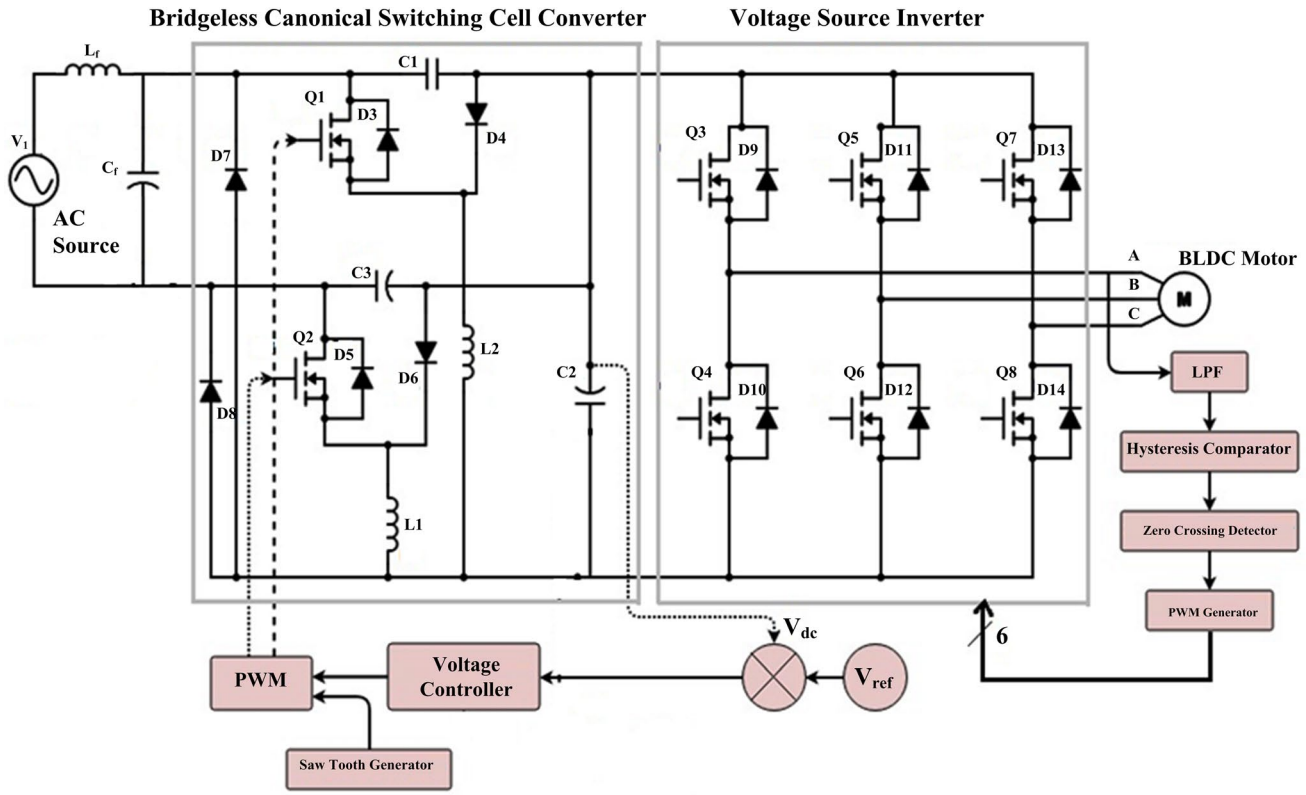

Fig. 8 Circuit diagram of BL-CSCC

2.7 BL-CSCC

Here the BL-CSC converter is sketched to operate in DICM. That is, the inductors are L1 and L2, the switching time is constant. Here, using different operational methods, for the NHC and PHC of the supply voltage, displays the complete transition period. The three modes are as follows:

Mode 1 While the switch is turned on input inductor L1 via the diode D8 starts to charge, and the current iL1 expansions. The intermediate capacitor C1 initiates to discharge along the switch Q1. Therefore, the voltage minimizes in the intermediate capacitor Vc1. At the identical time, the DC-link voltage must be added to the V_{dc}.

Mode 2 When switch Q1 is turn off, the power saved in the inductor L1 is the DC connector through the diode D4 is discharged to the capacitor C2. Now the current iL1 is lessening. At the uniform time, in this way of manner, the voltage of the DC connection continues to increase. Now the intermediate condenser begins to charge the C1. Then the voltage Vc1 increases.

Mode 3 Since the current at the input inductor L1 becomes zero, its function is called the DCM. The intermediate condenser C1, is continuously holding the power, and keeps its charge. Alike behavior of the converter, the other − ve of the V_{sc} is felt for the half cycle (Fig. 8).

The input voltage is offer in the usual Eq. (1). The equation for the value of the voltage now appearing in the inductor and switch amalgamation is given in the equation under,

$$V_{i(t)} = \left| V_p \sin(\omega t) \right| \tag{36}$$

The output voltage V_{dc} of the BL-CSC converter is,

$$V_{dc} = \frac{DR}{(1 - DR)} V_i \tag{37}$$

The duty rate D_R (t) is depends on the required DC connection voltage and i/p voltage V_i (*t*).The equation of the instant value of the duty rate is,

$$D_R(t) = \frac{V_{dc}}{V_i(t) + V_{dc}} \tag{38}$$

$$D_R(t) = \frac{V_{dc}}{\left| V_p \sin(\omega t) \right| + V_{dc}} \tag{39}$$

By differentiating the VSI's DC connection voltage, the pace of BLDC's motor is controlled. So in the DC connection voltage V_{dc}, Instantaneous power P_{ins} is taken as a task of the linear of V_{dc}.

$$P_{ins} = \left(\frac{P_{mx}}{V_{dcmx}} \right) V_{dc} \tag{40}$$

The critical value of the i/p inductive L_{ci} is computed as follows:

$$L_{ci} = \frac{V_i(t) D_R(t)}{2 i_i(t) f_{sw}} = \frac{R_i D_R(t)}{2 f_{sw}} \tag{41}$$

$$L_{ci} = \left(\frac{V_{sc}^2}{P_{ins}} \right) \frac{D_R(t)}{2 f_{sw}} \tag{42}$$

Estimation of the minimum critical value of the i/p inductor,

$$L_{cimn} = \left(\frac{V_{scmn}^2}{P_{mx}} \right) \frac{D_R(t)}{2 f_{sw}} \tag{43}$$

The equation for intermediate capacitance C1 and C2,

$$C1 = C2 = \frac{V_{dc} D_R(t)}{\Delta V_{ic}(t) f_{sw} R_{le}} \tag{44}$$

$$C1 = C2 = \frac{V_{dc} D_R(t)}{\eta f_{sw} R_{le} \left[V_i(t) + V_{dc} \right]} \tag{45}$$

where η = permitted ripple voltage, R_{le} = emulated load resistance and $V_{ic}(t)$ = intermediate capacitor's voltage.

The value of the intermediate condenser ripple is computed at the topmost value. The equation is given below,

$$C1 = C2 = \frac{V_{dcmx} D_R(t)}{\eta f_{sw} R_{le} \left[\sqrt{2} V_{scmx}(t) + V_{dc} \right]} \tag{46}$$

The equation of the value of the DC coupling capacitor,

$$C_{dc} = \left(\frac{P_{ins}}{V_{dc}} \right) \frac{1}{2 \omega \kappa V_{dc}} \tag{47}$$

2.8 Different Types of Driver System Control

2.8.1 Reference Voltage Generator (RVG)

A reference DC voltage that definition of V_{dc} is generated by a RVG; this is equivalent to the specific reference speed of the BLDC motor, To create the voltage error signal to be supplied to the speed controller, this voltage is differentiated to the perceived DC connection voltage. The reference voltage is produced by multiplying the voltage constant K_V of the BLDC motor with the reference speed.

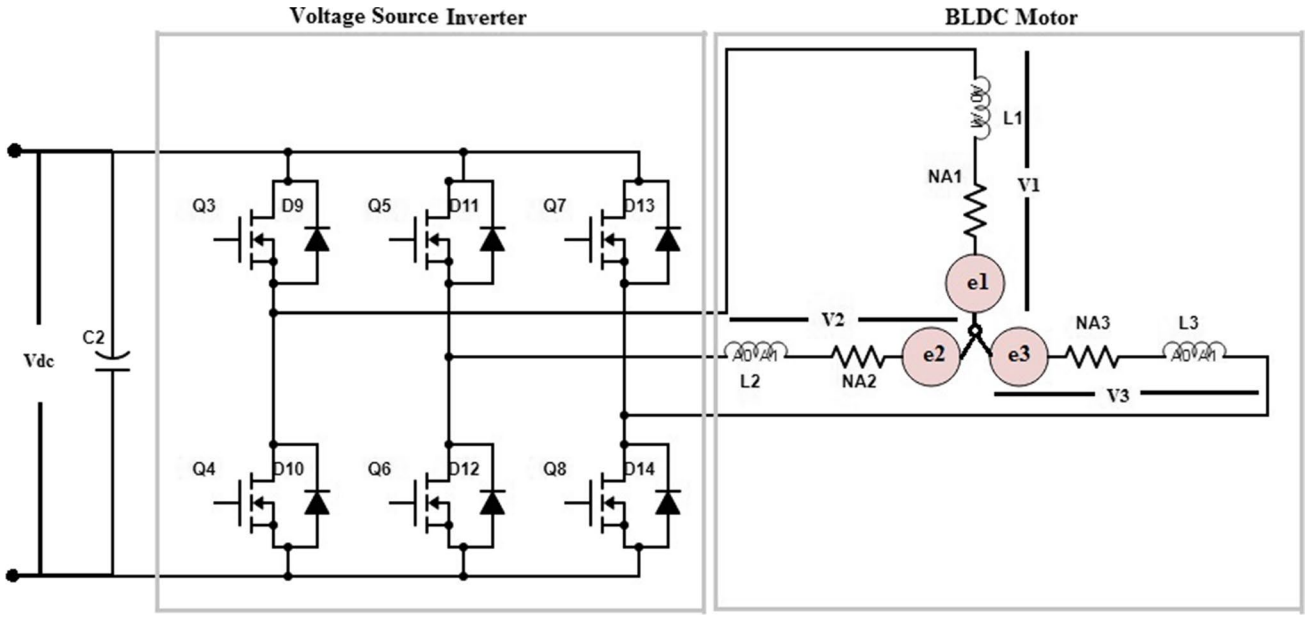

Fig. 9 VSI circuit diagram

2.8.2 Speed Controller (SC)

Then the voltage error signal is furnished to the SC. This is for creating a controlled output for the PWM generation level, proportional integral controller. Equation for controller output signal $V_{CO}(k)$ and voltage error signal $V_{ER}(k)$,

$$V_{ER}(k) = V'_{dc}(k) - V_{dc}(k) \tag{48}$$

$$V_{CO}(k) = V_{CO}(k-1) + K_{pg}\left[V_{ER}(k) + V_{ER}(k)\right] + K_{ig}V_{ER}(k) \tag{49}$$

where K_{pg} = proportional gain constants, K_{ig} = integral gain constants.

2.8.3 PWM Generator

A constant frequency differential duty rate PWM the controlled release of the speed controller by a PWM generator, is created by comparing with a high-frequency saw-tooth generator.

If $m_d(t) < V_{CO}(k)$, Then S1 = S2 = 1, else S1 = S2 = 0. Where, S1, S2 = switch.

2.9 BLDC Motor

The dynamic modeling of the BLDC motor is rule by the equations given below. A phase voltage is given below; V_k refers to V1, V2, and V3.

$$V_k = R_p.i_p + T_{dp}.\lambda_f + e_k \tag{50}$$

$$V_k = V_{pm} - V_{nm} \tag{51}$$

where, T_{dp} = time differential operator, R_p = resistance per phase, i_p = phase current, e_k = back emf, λ_f = flux linkages, V_{pm} = phase at the mid point, V_{nm} = neutral at the mid point.

Flux connections are denoted by the equation below,

$$\lambda_f = L_{Self} * i_p - L_M\left(i_q + i_r\right) \tag{52}$$

where L_{Self} = self-inductance, L_M = mutual inductance, If 'p' represents phase '1', then 'q' and 'r' represent the phases '2' and '3', respectively, and vice versa (Fig. 9).

The equation for the stator star-coupled three-phase torque at BLDC Motor,

$$\sum i_p = 0 \tag{53}$$

Here, substitute Eq. (53) in Eq. (52), so the equation of flux inductance is,

$$\lambda_f = \left(L_{Self} + L_M\right) i_p \tag{54}$$

The phase current calculate by using (50) and (54) are derived as,

$$T_{dp}i_p = \frac{V_1 - i_p R_p - e_1}{(L_{Self} + L_M)} \tag{55}$$

The sum of the expanded electromagnetic field of the BLDC motor,

$$T_{em} = \sum \frac{e_1 i_p}{\omega_{rs}} \tag{56}$$

where T_{em} = electromagnetic Torque, ω_{rs} = rotor speed electrical.

Since the induced EMFs are null, this disclosure of torque faces computational difficulty at zero speeds. So by exposing the back EMF as an operation of radar status angle, it is reorganized, so it can be noted as:

$$e_1 = k_{be} f_r(\theta)\omega_{rs} \tag{57}$$

where k_{be} = back EMF constant, $f_r(\theta)$ = functions of rotor position.

Substituting (57) into (56),

$$T_{em} = k_{be} \sum f_r(\theta) i_p \tag{58}$$

Equation of torque,

$$T_{em} = T_{Load} + C_f \omega_{rs} + M_i \left(\frac{2}{P_n}\right) T_{dp}\omega_{rs} \tag{59}$$

where T_{Load} = load torque, C_f = friction coefficient, M_i = moment of inertia, P_n = number of poles.

The Eq. (60) is used with Eq. (59) to find the torque time derivative. So the equation is,

$$T_{dp}\omega_{rs} = \frac{T_{em} - T_{Load} - C_f \omega_{rs}}{M_i \left(\frac{2}{P_n}\right)} \tag{60}$$

To avoid imbalance in the voltage utilized, the potential of the neutral terminal with zero energy must be considered. Equation (52) must be substitute in Eq. (51), the equation for as sum of the three phases,

$$\sum V_{pm} = R \sum i_p + \left(L_{Self} + L_M\right) T_{dp} \sum i_p + \sum e_1 \tag{61}$$

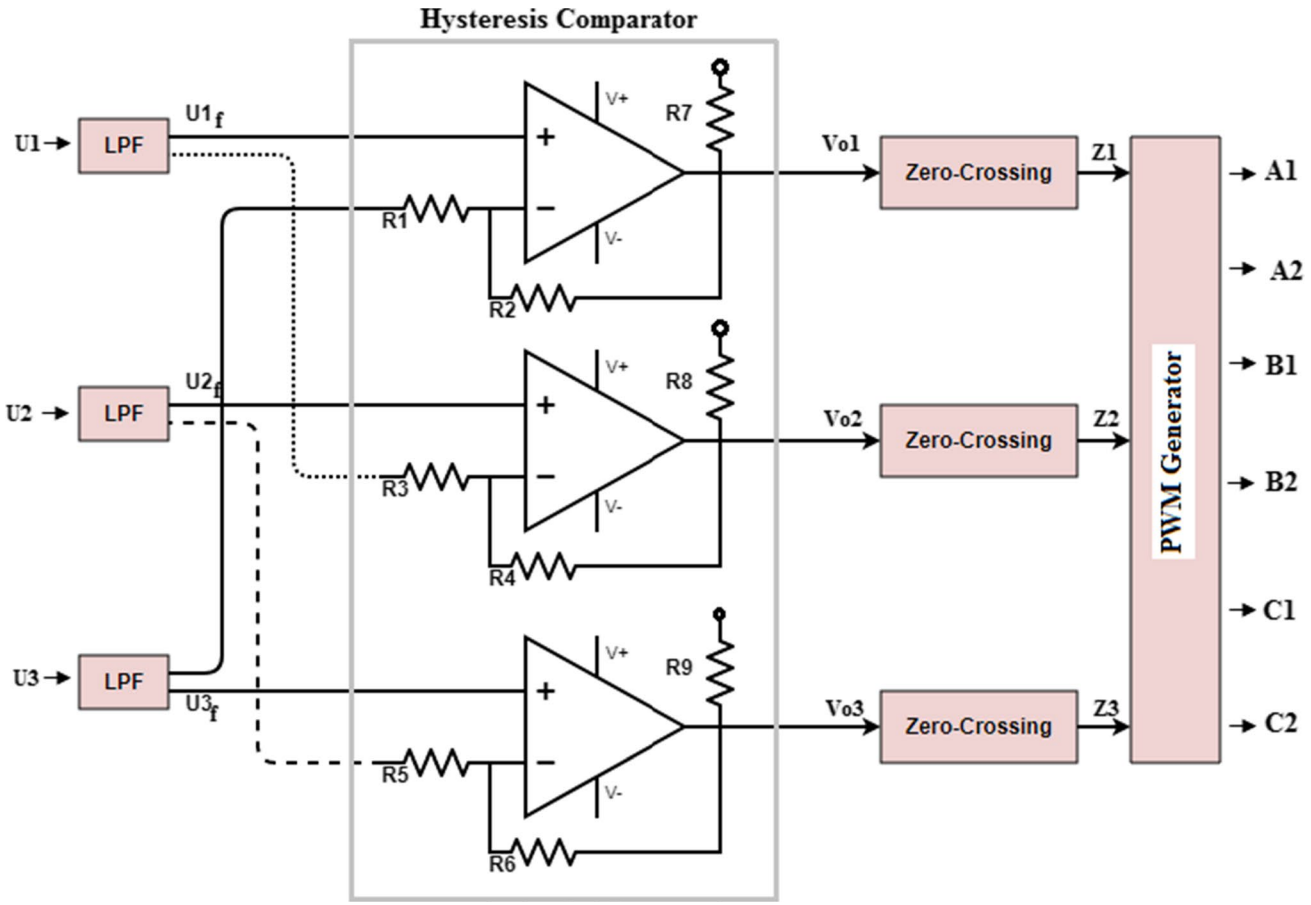

Fig. 10 Hysteresis comparator circuit diagram

Substituting Eq. (54) in (62) obtains,

$$\sum V_{pm} - 3V_{nm} = \sum e_1 \tag{62}$$

$$V_{\mathrm{nm}} = \frac{\sum V_{\mathrm{pm}} - \sum e_1}{3} \tag{63}$$

The equation of the rotor spot derivative of the BLDC motor,

$$P_{\mathrm{r}}(\theta) = \omega_{\mathrm{rs}} \tag{64}$$

where Eqs. (56), (61) and (65) regarded the equation current, speed and rotor position.

2.10 Voltage Source Inverter

Under is the sum for the release of the VSI for phase '1',

$$\text{For} \quad \mathrm{S1} = 1 \rightarrow \mathrm{V1_O} = \left(\frac{V_{\mathrm{dc}}}{2}\right) \tag{65}$$

$$\text{For} \quad \mathrm{S2} = 1 \rightarrow \mathrm{V1_O} = -\left(\frac{V_{\mathrm{dc}}}{2}\right) \tag{66}$$

$$\text{For} \quad \mathrm{S2} = 0 \rightarrow \mathrm{V1_O} = 0 \tag{67}$$

The ON and OFF conditions for S2 and S1 are, respectively, 1 and 0.

2.11 Sensorless Control Utilizing Terminal Voltage Sensing System

2.11.1 Terminal Voltage Sensing System(TVSS)

The hysteresis comparator with zero cross-detection technique achieves TVSS. In this it has the LPF of controlling the frequency ripples that are subject to high variations. At high speeds, there are comparators to compensate for the phase straggle of the Terminal Voltage (TV). In this condition; the motor neutral point voltage information is not used. Then perceive the 3 phase TV, each of the three phase TV essential a LPF to subdue high switching frequency noise or ripple. Since only 2 phases of the BLDC motor are running at any given time, during the open phase, back-EMF can be simplified from its TV.

During the two-phase abduction, the only variation betwixt the back EMF and its TV is, stator impedance is the voltage drop, and this may be less, differentiate to the DC voltage. Therefore the waveform of the TV is nearly the similar as that of the back EMF. TV can be utilized to discover the change points of the BLDC motor substitute of back EMF (Fig. 10).

2.11.2 LPF

To repress immoderate switching noise or ripples, each of the three phase terminal voltages is sustain to a LPF. Therefore, to eliminate excessive harmonics in phase terminal voltages caused by inverter switching, three LPF are used here.

2.11.3 Hysteresis Comparator and Zero Cross Detection

To determine the correct transmission line of the inverter according to the radar position, and to compensate for the backlash of back EMF due to LPF, the hysteresis comparator is used. At terminal voltages, with these, the output changes caused by high frequency distortion can be prevented. Three hysteresis comparators are used here. The output of each terminal voltage emitted from the LPF is provided to the comparator.

As the rotor pace improves, the percentage contribution becomes phase lag for the whole duration. This setback would disarrange the back EMF arrangement. And at high speeds, transmission can cause serious problems. The phase lag of the transmission, in such a movement significant pulse torques may develop. The release of the hysteresis comparator is given to the zero crossover detector.

From three-stage hysteresis comparators, outputs become three transmission signals, then there are the six step PWM signals, this means that six gating signals are generated by the PWM method. Inverter switches control the boom and compassion of the signals along the margin of the transmission. Gating signaling is derived from hysteresis comparators and from each exchange event. By selecting Sensing and PWM correctly, without using the motor's unprejudiced point voltage data, back EMF signals can be obtained directly from the motor TV.

3 Results and Discussion

In this section, the comparative analysis of the 5 bridgeless converters reported in the top section is shown. In that comparison, using the five types of parameters are compared. They are Speed, THD, DPF, PF and I_s.Below you will find how these five parameters are calculated.

Here speed values are taken from 450 to 2350 rpm and the input voltage values are taken from 90 and 290 V.

3.1 THCD (total harmonic current distortion)

THCD is the measure of existing compliant distortion. It is clarify as the energy of the foundational frequency current of the total of the energies of all the harmonic current elements.

$$\text{THCD} = \frac{\sqrt{I_{D2}^2 + I_{D3}^2 + I_{D4}^2 \cdots + I_{Dn}^2}}{I_{D1}} \times 100\% \quad (68)$$

$$\text{Crest factor (CF)} = \frac{|I_P|}{I_{rms}} \quad (69)$$

$$I_{rms} = \sqrt{I_{D1}^2 + I_{D2}^2 + I_{D3}^2 \cdots + I_{Dn}^2} \quad (70)$$

where I_{Dn} = individual HCD values, I_{D1} = Fundamental HCD value, I_{D2} = Second HCD values.

3.2 DPF (Displacement Power Factor)

At the base-line frequency, the DPF is established as the PF due to the phase change in V and I.

$$\text{DPF} = \cos(\theta) \quad (71)$$

Here, θ is the phase angle betwixt the base current and the voltage.

3.3 PF (Power Factor)

The proportional betwixt apparent power and true power. So the calculation of PF is,

$$\text{PF} = \frac{\text{True power}}{\text{Apparent power}} \quad (7)$$

The multiply of the rms I and the rms V is called apparent power.

Table 1 The value of THCD and DPF of bridgeless converters

V_{dc} (V)	Speed (rpm)	THD of I_s (%)					DPF				
		BL-LC	BL-CC	BL-BBC	BL-ZC	BL-CSCC	BL-LC	BL-CC	BL-BBC	BL-ZC	BL-CSCC
90	450	6.01	3.29	4.85	5.21	7.02	0.9990	0.9991	0.9923	0.9952	0.9989
110	650	5.84	3.11	4.74	4.98	6.84	0.9991	0.9991	0.9943	0.9959	0.999
130	850	5.67	2.89	4.63	4.91	6.67	0.9992	0.9992	0.9959	0.9974	0.9993
150	1040	5.5	2.85	3.94	4.83	6.50	0.9993	0.9993	0.9979	0.9979	0.9995
170	1230	5.33	2.81	3.37	4.75	6.33	0.9994	0.9994	0.9981	0.9983	0.9996
190	1420	5.16	2.77	3.2	4.62	6.16	0.9995	0.9995	0.9984	0.9988	0.9996
210	1610	4.99	2.73	2.9	4.41	5.98	0.9996	0.9996	0.9987	0.9993	0.9997
230	1790	4.82	2.62	2.6	4.29	5.81	0.9997	0.9997	0.9993	0.9995	0.9998
250	1980	4.65	2.51	2.3	4.04	5.64	0.9998	0.9998	0.9997	0.9998	0.9999
270	2170	4.48	2.4	1.84	3.83	5.46	0.9999	0.9999	0.9998	0.9999	1
290	2350	4.31	2.29	1.46	3.59	5.29	1	1	0.9998	1	1

Table 2 The value of PF and I_S of bridgeless converters

V_{dc} (V)	PF					I_s (A)				
	BL-LC	BL-CC	BL-BBC	BL-ZC	BL-CSCC	BL-LC	BL-CC	BL-BBC	BL-ZC	BL-CSCC
90	0.9950	0.9975	0.9922	0.9947	0.9915	0.835	0.649	1.124	1.572	2.334
110	0.9953	0.9978	0.9941	0.9954	0.9924	0.985	0.785	1.236	1.756	2.452
130	0.9956	0.9981	0.9956	0.997	0.9933	1.135	0.929	1.335	1.945	2.570
150	0.9959	0.9983	0.9965	0.9975	0.9942	1.285	1.071	1.463	2.137	2.688
170	0.9962	0.9985	0.997	0.9979	0.9951	1.435	1.215	1.591	2.335	2.806
190	0.9965	0.9985	0.9976	0.9983	0.996	1.585	1.359	1.781	2.527	2.924
210	0.9968	0.9987	0.9981	0.9987	0.9969	1.735	1.512	1.968	2.719	3.042
230	0.9971	0.9989	0.9985	0.9992	0.9978	1.885	1.662	2.281	2.911	3.160
250	0.9974	0.9991	0.9992	0.9996	0.9987	2.035	1.815	2.596	3.103	3.278
270	0.9977	0.9993	0.9993	0.9998	0.9996	2.185	1.972	3.256	3.295	3.396
290	0.998	0.9994	0.9993	1	1	2.335	2.145	3.915	3.487	3.510

3.4 I_S (Supply Current)

The I_S is the load currents supplied to the loads by the constant current, switching current and outputs.

The THCD tells how much distortion of the current (I_d) is there. If the I_d is elevated, the wave of the current is not understandable. Thus, it is hugely tough to perfectly discover the value of the current wave. Therefore, in this contrast, the lowest THCD value is there only for the BL-CC. This is shown in Tables 1, 2.

This DPF expand the lifetime of the equipment. Hence, BL-CC converter has the best DPF value.

This PF reduces the heat dissipation of the apparatus and improves the life of the device. The converter with such a better PF is BL-CC. By varying the values of these parameters, BL-CC has a very high efficiency, so this BL-CC is the better of these five converters.

4 Conclusion

Using the proposed BLDC Drive method, generating results obtained for sensorless speed control, the isolated AC to DC converter has manifested the improve of power quality at AC mains. The hysteresis comparator technique has exceptional performance and sensing system. Moreover, the wider motor speed limits instantly, that means making it stable. Here is there a very important advantage of separating the inverter transmission from the speed control area. This enables the smooth and clean operation of the movement. The switch pattern required for the inverter is obtained using the terminal emf using hysteresis comparator. The increase in cost due to rotor position sensors is overcome by using this method and the noise undulation in the back emf can be reduced using this comparator technique. Also usage of sensorless techniques is highly recommended in rugged environments with wide range of operations and applications. Harmonics is been controlled by the proposed method, and therefore, various international standards of power quality improvement are achieved.

References

1. Bist, V.; Singh, B.: An adjustable speed PFC bridgeless buck-boost converter fed BLDC motor drive. IEEE Trans. Ind. Electro. **61**(6), 2665–2677 (2014)
2. Singh, B.; Bist, V.: A BL-CSC converter-fed BLDC motor drive with power factor correction. IEEE Trans. Ind. Electron. **62**(1), 172–183 (2015)
3. Singh, B.; Bist, V.: Improved power quality bridgeless Cuk converter fed brushless DC motor drive for air conditioning system. IET Power Electron. **6**(5), 902–913 (2013). https://doi.org/10.1049/iet-pel.2013.0050
4. Chandra, A.; Al-Haddad, K.: An adjustable speed PFC bridgeless-SEPIC fed brushless DC motor drive. In: 2015 IEEE Energy Conversion Congress and Exposition (ECCE), Conference Paper (2015)
5. Singh, P.K.; Singh, B.: BLDC motor drive based on bridgeless landsman PFC converter with single sensor and reduced stress on power devices. IEEE Trans. Ind. Appl. **54**(1), 625–635 (2018)
6. Singh, B.; Chandra, A.: Power factor correction in bridgeless-Luo converter-fed BLDC motor drive. IEEE Trans. Ind. Appl. **51**(2), 1179–1188 (2015)
7. Singh, B.; Bist, V.: A PFC based BLDC motor drive using a bridgeless zeta converter. In: IECON 2013—39th annual conference of the IEEE industrial electronics society, conference paper (2013)
8. Chun, T.-W.; Tran, Q.-V.: Sensorless control of BLDC motor drive for an automotive fuel pump using a hysteresis comparator. IEEE Trans. Power Electron. **29**(3), 1382–1391 (2014)
9. Yang, L.; Zhu, Z.Q.: Safety operation area of zero-crossing detection based sensorless high speed BLDC motor drives. In: 2019 IEEE International Electric Machines & Drives Conference (IEMDC) (2019)
10. Mathan, K.; Kumar, P.M.; Panchatcharam, P.; Manogaran, G.; Varadharajan, R.: A novel Gini index decision tree data mining method with neural network classifiers for prediction of heart disease. Des. Autom. Embed. Syst. **22**(3), 225–242 (2018)
11. Singh, S.; Singh, B.: Power quality improved PMBLDCM drive for adjustable speed application with reduced sensor buck-boost PFC converter. In: 4th International Conferences Emerging Trends in Engineering and Technology (ICETET), pp. 180–184 (2011)
12. Gopalarathnam, T.; Toliyat, H.A.: A new topology for unipolar brushless DC motor drive with high power factor. IEEE Trans. Power Electron **18**(6), 1397–1404 (2003)
13. Huber, L.; Jang, Y.; Jovanovic, M.M.: Performance evaluation of bridgeless PFC boost rectifiers. IEEE Trans. Power Electron **23**(3), 1381–1390 (2008)
14. Fardoun, A.A.; Ismail, E.H.; Al-Saffar, M.A.; Sabzali, A.J.: New "real" bridgeless high efficiency AC-DC converter. In: 2012 Twenty-Seventh Annual IEEE Applied Power Electronics Conference and Exposition (APEC), pp. 317–323 (2012)
15. Parthasarathy, P.; Vivekanandan, S.: A typical IoT architecture-based regular monitoring of arthritis disease using time wrapping algorithm. Int. J. Comput. Appl. **42**(3), 222–232 (2020)
16. Fardoun, A.A.; Ismail, E.H.; Sabzali, A.J.; Al-Saffar, M.A.: New efficient bridgeless Cuk rectifiers for PFC applications. IEEE Trans. Power Electron. **27**(7), 3292–3301 (2012)
17. Fardoun, A.A.; Ismail, E.H.; Sabzali, A.J.; Al-Saffar, M.A.: A comparison between three proposed bridgeless Cuk rectifiers and conventional topology for power factor correction. In: 2010 IEEE International Conference on Sustainable Energy Technologies (ICSET), pp. 1–6 (2010)
18. Parthasarathy, P.; Vivekanandan, S.: A numerical modelling of an amperometric-enzymatic based uric acid biosensor for GOUT arthritis diseases. Inf Med Unlocked **12**, 143–147 (2018)
19. Sabzali, A.J.; Ismail, E.H.; Al-Saffar, M.A.; Fardoun, A.A.: New bridgeless DCM Sepic and Cuk PFC rectifiers with low conduction and switching losses. IEEE Trans. Ind. Appl. **47**(2), 873–881 (2011)
20. Kumar, P.M.; Lokesh, S.; Varatharajan, R.; Babu, G.C.; Parthasarathy, P.: Cloud and IoT based disease prediction and diagnosis system for healthcare using Fuzzy neural classifier. Futur. Gener. Comput. Syst. **86**, 527–534 (2018)